## COMMUNICATION

Check for updates

# Controlled adhesion, membrane pinning and vesicle transport by Janus particles†

Eleanor J. Ewins, [ID] ‡*[a] Koohee Han, [ID] §[b] Bhuvnesh Bharti, [ID] ¶[b] Tom Robinson, [ID] [a] Orlin D. Velev [ID] [b] and Rumiana Dimova [ID] *[a]

**The interactions between biomembranes and particles are key to many applications, but the lack of controllable model systems to study them limits the progress in their research. Here, we describe how Janus polystyrene microparticles, half coated with iron, can be partially engulfed by artificial cells, namely giant vesicles, with the goals to control and investigate their adhesion and degree of encapsulation. The interaction between the Janus particles and these model cell membrane systems is mediated by electrostatic charge, offering a further mode of modulation in addition to the iron patches. The ferromagnetic particle coatings also enable manipulation and transport of the vesicles by magnetic fields.**

Interactions of particles with biomembranes are widely studied due to their relevance in multiple current and potential applications, such as in medical imaging,[1] or as antimicrobial agents,[2] or to understand the negative environmental impact of microplastics.[3] In order to take full advantage of these applications, it is important to understand the underlying mechanisms and parameters that govern the adhesion and engulfment of particles by membranes. In cells, this process is referred to as endo- or phagocytosis. Model membrane systems are commonly implemented for studying such processes.[4] Among these systems are giant unilamellar vesicles (GUVs),[5] which mimic the cell size and the curvature of the plasma membrane without the compositional complexity of live cells (which includes a wide variety of lipid species, proteins or the associated

cytoskeleton).[6] When investigating the parameters that dictate particle–membrane interactions, one vital aspect to consider is the role of the particle properties on the interaction potentials. For example, previous studies have examined how size, shape and surface chemistry impact the interactions of particles with cells[7] or mimetic systems.[4k,8] What has yet to be explored experimentally is non-receptor mediated interactions between membranes and particles with surface asymmetry.

By using micron-sized Janus particles with two regions of distinctly different surface properties, we investigate to what extent spatially varied surface properties govern the microsphere adhesion and engulfment by GUVs. Such anisotropic particles are of particular interest as they combine two different and sometimes incompatible properties within a single particle.[9] They also provide means to quantify rotational dynamics due to their broken symmetry,[4j] which could be a promising method to study particle endocytosis[10] or self-propelled guided transport and membrane deformation.[4j,k] We find that by spatially altering the particles' surface chemistry, we can control their adhesion and engulfment. We also make use of the iron oxide coating on the particle hemisphere to manipulate particle–vesicle pairs using an external magnetic field gradient.

To select a GUV–particle combination exhibiting adhesion, we first performed high-throughput screening with large unilamellar vesicles (LUVs) of different compositions. The LUVs were prepared *via* extrusion and incubated with particles of different surface chemistries, see Section S1.2 in the ESI.† LUVs were composed of DOPC with 40 mol% either DOPG (negative) or DOTAP (positive) to modulate the membrane charge, see ESI† for abbreviations and lipid structures. The microparticles used were polystyrene, either functionalised with sulphate or amine groups, resulting in negatively and positively charged surfaces respectively at neutral pH (here pH 7.45). The use of fluorescently labelled LUVs, containing 0.5 mol% Rh-DPPE, allowed for qualitative analysis of the relative affinity between the particle–vesicle combinations.

We observed a clear affinity of the positively charged LUVs to the negative polystyrene particles, see ESI,† Fig. S3. Subsequently,

[a] *Max Planck Institute of Colloids and Interfaces, 14476 Potsdam, Germany.*
 *E-mail: e.j.ewins@rug.nl, rumiana.dimova@mpikg.mpg.de*
[b] *Department of Chemical and Biomolecular Engineering, North Carolina State University, Raleigh, NC, 27695, USA*
† Electronic supplementary information (ESI) available. See DOI: 10.1039/d1cc07026f
‡ Current address: Department of Biochemistry, Groningen Institute of Biomolecular Sciences & Biotechnology, University of Groningen, The Netherlands.
§ Current address: Department of Chemical Engineering, Kyungpook National University, Daegu, Republic of Korea.
¶ Current address: Cain Department of Chemical Engineering, Louisiana State University, Baton Rouge, LA 70803, USA.

we investigated the interactions of positively charged GUVs (containing DOTAP) with uniform and Janus particles exposing a negative (sulphate) surface. The GUVs were prepared *via* electroformation (ESI,† Section S1.2) from DOPC, doped with 0–5 mol% DOTAP (above 5 mol% the GUV quality and yield was very poor) and 0.5 mol% Rh-DPPE in 200 mM sucrose. Adhesion to neutral membranes (0% DOTAP) was not observed. The negative charge of the uniform polystyrene particles is from surface sulphate groups.

Iron-patched Janus microspheres were prepared from the uniform particles *via* metal vapour deposition (see ESI,† Section S1.3)[11] resulting in a hemispherical patch of 5 nm of chromium and 20 nm of iron. Note that the iron patch transforms to iron oxide upon particle resuspension in an aqueous environment.[11] This patch appears darker in brightfield images, see Fig. S2C (ESI†).

Both the uniform and Janus particles were dispersed in hypertonic glucose solutions (see ESI,† Section S1 for details); particle incubation with the GUVs generates excess membrane area *via* osmotic deflation of the vesicles. We observed that this deflation step was necessary for particle engulfment to occur to any extent. Fig. 1 shows example images of the two samples; 5% DOTAP GUVs that, typically, completely engulf the uniform, negatively charged particles (Fig. 1A), whereas the Janus particles are partially engulfed (half-wrapped) exhibiting pinning of the membrane contact line (Fig. 1B). For the Janus particles, the region of the particle in contact with the membrane is the polystyrene half (light region on particle in Fig. 1B) and the iron-patched half (dark region) remains at the periphery and restricts engulfment. The complete engulfment of the uniform particles suggests strong adhesion of the membrane to the microsphere. This is corroborated by observations showing that the surface of Janus particles is only partially covered by LUVs, see Fig. S4 (ESI†).

These observations imply that the degree and energy of particle engulfment could be tuneable by altering the proportion of the particle surface that has a strong interaction with the membrane, here shown on half-coated (Janus) or uniform particles. We further investigated this concept by measuring how the penetration depth of the particles into vesicles varied, both as a function of the particle surface (uniform or Janus) and membrane charge (either 5 or 1% DOTAP). These results are displayed in Fig. 2, together with a sketch illustrating the definition of particle penetration depth, $d$, which is comparable to that introduced by Dietrich *et al.*,[12] who analysed the uptake of uniform particles. Normalisation of $d$ allows us to compare particles and vesicles of different sizes. The images in Fig. 1 show a "close-to-ideal" orientation of the vesicle–particle system, which directly reveals the penetration depth. However, the particles can also exhibit different positions with respect to the vesicle centre, and are typically located at the lower part of the GUV, making it nearly impossible to resolve $d$ from projected images. We thus further develop the approach in ref. 12 taking advantage of the improved resolution of confocal microscopy, especially in the axial direction, see ESI,† Section S3.

The analysis of multiple interactions shows that uniform particles penetrate further into the vesicles than Janus particles do (Fig. 2), as expected from the observations in Fig. 1. The metallic regions supposedly repel the membrane or do not contribute a significant energy gain if the membrane would continue deforming to wet this part of the surface. Therefore, the wetting of the particle surface stops and the particle only partially penetrates into the vesicle. The contact line is pinned
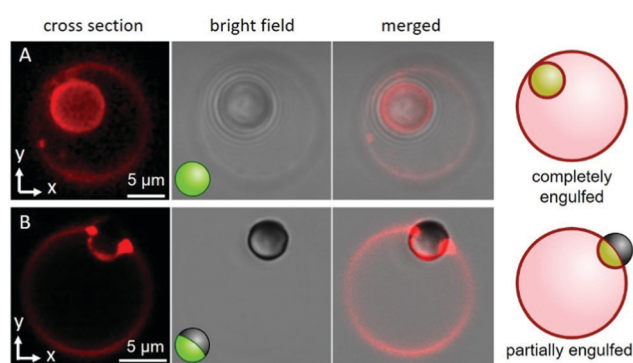


Fig. 1 Confocal cross section and bright-field microscopy images of 5% DOTAP GUVs (red fluorescence) in contact with microparticles with uniform (A) and Janus (B) surface chemistries. (A) A 6 μm negatively charged polystyrene particle is completely engulfed by the GUV. (B) A 4 μm Janus particle, half negatively charged polystyrene and half with a thin coating of iron oxide, is partially engulfed by the GUV. The contact line of the adhered vesicle approximately corresponds to the iron oxide-coated region of the particle surface, which can be seen in the brightfield image as the darker region (orientated away from the vesicle surface). The sketches summarise these observations.
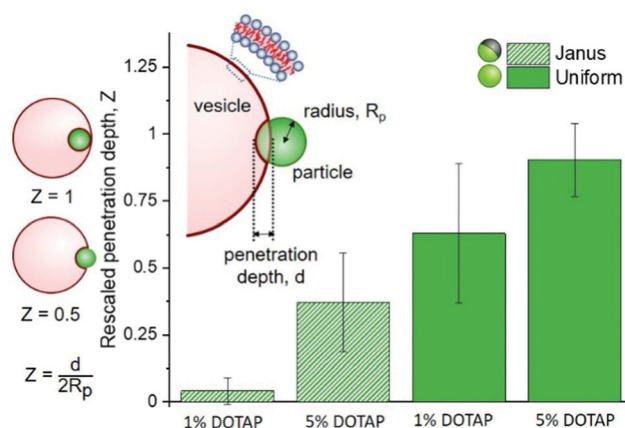


Fig. 2 Penetration depths of Janus and homogeneous particles into GUVs composed of DOPC with 1 or 5% DOTAP (positively charged). Penetration depth $d$ sketched in the inset is normalised by the particle diameter $2R_p$, so that different sized particles can be directly compared. The sketches on the left are representative of rescaled penetration depths of $Z = 0.5$ and $Z = 1$. Janus particles, with half of their surface coated in metal, do not penetrate further than their radial depth into the vesicles ($Z < 0.5$), whereas homogeneous particles penetrate further. Between the two particle types, both particles penetrate further into more positively charged membranes (an effective increase in adhesion energy). Numbers of analyzed vesicle–particle pairs: 1% DOTAP, Janus $n = 8$, uniform $n = 7$; 5% DOTAP, Janus $n = 10$, uniform $n = 4$. The vesicle diameters were in the range of 10–42 μm, and the particle diameters were 3.7–4.05 μm (Janus) and 5.8–6.3 μm (uniform).

at the boundary between the polystyrene and iron oxide. Based on the data shown in Fig. 2, we can also see that there isn't any single definitive penetration depth for each condition. This is most likely due to the challenges that arise from GUV and particle preparation: (i) for GUVs produced from a lipid mixture, it has been shown that the individual vesicle compositions vary,[13] so does the vesicle size relative to that of the particles. (ii) Vesicles with similar sizes can exhibit variable excess area for wrapping the particles. (iii) The surface chemistry of the polystyrene part of the Janus particles may differ from that of the homogeneous particles because of preparation steps (see ESI,† Section S1.3). (iv) Variation in the membrane spontaneous curvature expected due to charge asymmetry[13] has been predicted to play a crucial role in particle engulfment.[14]

For both uniform and Janus particles the penetration depths have a dependence on the membrane charge (percentage of positively charged DOTAP, see Fig. 2); essentially, increasing the adhesion energy between the particle and the vesicle results in increased particle penetration. This process is seemingly governed by charge. To further investigate this, we observed the effects of increased ionic strength (150 mM NaCl) on adhesion of LUVs with DOTAP to uniform particles.

Fig. 3A shows images of particles with adhered LUVs in the presence and absence of salt, see also Fig. S6, ESI.† To assess the effect of salt, we quantified the fluorescence intensity of the particles; see Fig. S7 (ESI†). In 150 mM NaCl, which is expected to screen the charges, the intensity of the adhered LUVs is roughly 1.8 times lower than that of the samples containing only sugars (0 mM NaCl), Fig. 3C; the scatter in fluorescence intensity values is possibly due to the small size variation between particles, as all particles are measured at the same distance from the glass surface. The results demonstrate that

the interactions depend on electrostatics, in correlation with our observations of increased penetration depths in GUVs with a higher DOTAP content.

However, these interactions are not only electrostatic, as we still detect some LUV fluorescence on the particles in the presence of salt. Fig. 3B includes a sketch depicting different possible configurations of the LUV lipids and membrane at the particle surface: (i) docked LUVs (single adhered LUVs appear to produce stronger signal; see Fig. S8, ESI†); (ii) supported lipid bilayer (shown to form when LUVs adhere to silica particles and collapse[15]); and (iii) frustrated lipid monolayer adsorbed onto the hydrophobic regions of the latex surface as speculated by Dietrich et al.[12]

In addition to providing a region with a lower adhesion energy, the iron oxide patch on the Janus particles also attributes magneto-responsiveness.[16] The particles move towards regions of higher magnetic field intensity (magnetophoresis). This is widely used with uniform magnetic particles in cell sorting protocols.[17] Indeed, we observe magnetophoresis of the Janus particle–vesicle complex in the presence of a magnetic field (Fig. 4), see ESI for setup details.† GUVs were prepared from DOPC/DOTAP 95/5 mol%. When the source of the magnetic field is located to the lower left of the chamber, the particle–vesicle pair moves in this direction (Fig. 4A). Conversely, when the magnet is moved to the upper right corner of the chamber, the same particle–vesicle pair changes direction (Fig. 4B). The particle remained adhered to the GUV, and it was possible to repeat similar manipulations with further particle–vesicle pairs, where the distance traversed was
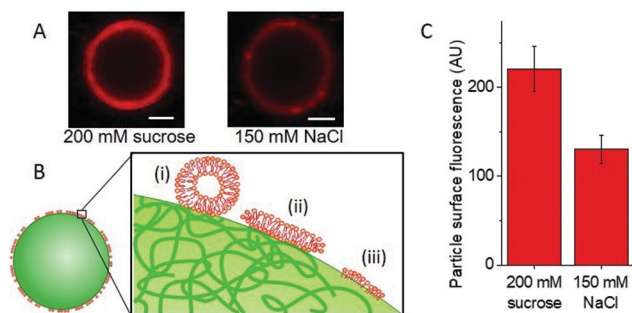


Fig. 3 Effects of salt on the adhesion of positively charged membranes to negatively charged uniform particles. (A) LUVs (100 nm) composed of DOPC/DOTAP/Rh-DPPE 94.5/5/0.5, adhere to negatively charged polystyrene 6 μm particles to varying extents depending on the salt concentration in the solution, as deduced from confocal scans (scale bars: 2 μm). (B) The sketch (not to scale) represents possible reorganization of the LUV membrane (red) upon contact with the particle surface (green) leading to non-uniform fluorescence over the particle: (i) LUV adhesion, (ii) vesicle rupture and formation of a supported bilayer, or (iii) restructuring to a monolayer-like structure adhered to more hydrophobic patches on the particle surface. (C) In the presence of sugars, the fluorescence intensity on the particle surface is roughly 1.8 times higher; the presence of salt partially screens the electrostatic LUV-particle interactions. The analysis is performed on 10 particles for each condition.
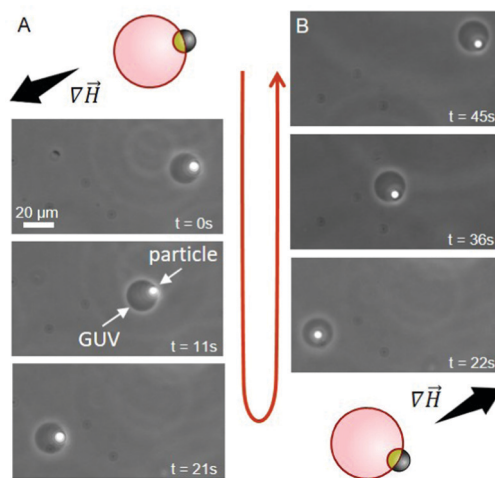


Fig. 4 Time sequence demonstrating the transport of a GUV (dark circle) via manipulation with an adhered Janus particle (white spot) under magnetic field gradient (∇H⃗); phase-contrast microscopy, see also ESI,† Movie S1. The dense particle has sedimented to the lower half of the vesicle (out of focus, appearing inside), but it is outside the GUV. The schematic diagrams indicate the initial particle–vesicle configuration and the magnetic field gradient. (A) The magnet is located to the bottom left, causing the Janus particle to move towards higher field gradient. (B) The magnet is now located to the top right and the Janus particle moves towards this region. The particles are heavy and having both vesicle and particle in focus is not always possible.

comparable to the size of the observation chamber ($\approx$ 10 mm). Our approach of transporting vesicles by means of adsorbed Janus particles provides a facile and precise means of moving and sorting GUVs. The approach appears superior in terms of transporting the vesicles over large distances compared to mainly rotating them as shown previously.[18]

In conclusion, we demonstrated the ability to control the extent of particle engulfment by membranes using Janus particles with regions of different affinities for the GUV membrane. We also show that the particle iron oxide coating provides enhanced capabilities for vesicle transport *via* magnetophoresis.

The degree of penetration depends on both particle surface asymmetry and lipid composition. This is coupled with a decrease in LUV adhesion in the presence of salt, suggesting that this system could be finely tuned to provide the desired degree of particle adhesion and penetration.

The use of Janus particles as a means to separate cell-like objects provides multiple opportunities for further development. The anisotropic surface could be used to limit the cells' exposure to the damaging iron oxide,[19] by creating regions of higher and lower affinity with the membrane. The exposed, non-binding region of the particle could also be functionalised so as to undergo surface reactions, as another means for generating self-propulsion.[20] The selective adhesion demonstrated here could also be used as a template for spatially confined lipid sorting, as demonstrated earlier.[18] The controlled and directional force applied to GUVs could be used for quantitative characterization of the membrane stiffness and moduli. This can be achieved both by the magnetic pull-off and torque. One could also consider a potential use of the entire vesicle–particle ensemble as a drug delivery system, with the manoeuvrability provided by the iron oxide patch, the lipids ensuring biocompatibility and the vesicles serving as a drug transporter.

## Conflicts of interest

There are no conflicts to declare.

## References

1 X. Mulet, B. J. Boyd and C. J. Drummond, *J. Colloid Interface Sci.*, 2013, **393**, 1–20.
2 (*a*) L. Wang, C. Hu and L. Shao, *Int. J. Nanomed.*, 2017, **12**, 1227–1249; (*b*) G. Ren, D. Hu, E. W. C. Cheng, M. A. Vargas-Reus, P. Reip and R. P. Allaker, *Int. J. Antimicrob. Agents*, 2009, **33**, 587–590.
3 M. Cole, P. Lindeque, C. Halsband and T. S. Galloway, *Mar. Pollut. Bull.*, 2011, **62**, 2588–2597.
4 (*a*) A. S. V. L. C. Peetla, *Mol. Pharmaceutics*, 2009, **6**, 1264–1276; (*b*) K. L. Chen, *Environ. Sci. Technol.*, 2014, **48**, 873–880;

(*c*) H. Kettiger, G. Québatte, B. Perrone and J. Huwyler, *Biochim. Biophys. Acta*, 2016, **1858**, 2163–2170; (*d*) I. Koltover, J. O. Rädler and C. R. Safinya, *Phys. Rev. Lett.*, 1998, **82**, 1991–1994; (*e*) E. Ewins, R. B. Lira, W. Y. Zhang, J. Y. Yuan, M. Antonietti, T. Robinson and R. Dimova, *Adv. Sci.*, 2019, **6**; (*f*) C. van der Wel, D. Heinrich and D. J. Kraft, *Biophys. J.*, 2017, **113**, 1037–1046; (*g*) S. Li and N. Malmstadt, *Soft Matter*, 2013, **9**, 4969; (*h*) H. T. Spanke, R. W. Style, C. François-Martin, M. Feofilova, M. Eisentraut, H. Kress, J. Agudo-Canalejo and E. R. Dufresne, *Phys. Rev. Lett.*, 2020, **125**, 198102; (*i*) C. Van Der Wel, N. Bossert, Q. J. Mank, M. G. T. Winter, D. Heinrich and D. J. Kraft, *Langmuir*, 2017, 33; (*j*) V. Sharma, E. Azar, A. P. Schroder, C. M. Marques and A. Stocco, *Soft Matter*, 2021, **17**, 4275–4281; (*k*) H. R. Vutukuri, M. Hoore, C. Abaurrea-Velasco, L. van Buren, A. Dutto, T. Auth, D. A. Fedosov, G. Gompper and J. Vermant, *Nature*, 2020, **586**, 52–56; (*l*) A. H. Bahrami, R. Lipowsky and T. R. Weikl, *Phys. Rev. Lett.*, 2012, **109**, 188102.
5 (*a*) R. Dimova, S. Aranda, N. Bezlyepkina, V. Nikolov, K. A. Riske and R. Lipowsky, *J. Phys.: Condens. Matter*, 2006, **18**, 1151–1176; (*b*) P. Walde, K. Cosentino, H. Engel and P. Stano, *ChemBioChem*, 2010, **11**, 848–865; (*c*) R. Dimova and C. Marques, *The giant vesicle book*, CRC Press, 2019.
6 (*a*) Y. H. M. Chan and S. G. Boxer, *Curr. Opin. Chem. Biol.*, 2007, **11**, 581–587; (*b*) S. F. Fenz and K. Sengupta, *Integr. Biol.*, 2012, **4**, 982–995.
7 (*a*) B. D. Chithrani, A. A. Ghazani and W. C. W. Chan, *Nano Lett.*, 2006, **6**, 662–668; (*b*) S. E. A. Gratton, P. A. Ropp, P. D. Pohlhaus, J. C. Luft, V. J. Madden, M. E. Napier and J. M. DeSimone, *Proc. Natl. Acad. Sci. U. S. A.*, 2008, **105**, 11613–11618; (*c*) M. Wu, H. Guo, L. Liu, Y. Liu and L. Xie, *Int. J. Nanomed.*, 2019, **14**, 4247–4259; (*d*) J. Rejman, V. Oberle, I. S. Zuhorn and D. Hoekstra, *Biochem. J.*, 2004, **377**, 159–169.
8 (*a*) S. Zhang, A. Nelson and P. A. Beales, *Langmuir*, 2012, **28**, 12831–12837; (*b*) M. Bally, A. Gunnarsson, L. Svensson, G. Larson, V. P. Zhdanov and F. Höök, *Phys. Rev. Lett.*, 2011, **107**, 188103; (*c*) K. Shigyou, K. H. Nagai and T. Hamada, *Langmuir*, 2016, **32**, 13771–13777.
9 (*a*) S. Jiang, Q. Chen, M. Tripathy, E. Luijten, K. S. Schweizer and S. Granick, *Adv. Mater.*, 2010, **22**, 1060–1071; (*b*) A. Walther and A. H. E. Müller, *Soft Matter*, 2008, **4**, 663–668.
10 (*a*) Y. Gao and Y. Yu, *Langmuir*, 2015, **31**, 2833–2838; (*b*) Y. Gao and Y. Yu, *J. Am. Chem. Soc.*, 2013, **135**, 19091–19094.
11 B. Bharti, D. Rutkowski, K. Han, A. U. Kumar, C. K. Hall and O. D. Velev, *J. Am. Chem. Soc.*, 2016, **138**, 14948–14953.
12 C. Dietrich, M. Angelova and B. Pouligny, *J. Phys. II*, 1997, **7**, 1651–1682.
13 J. Steinkühler, P. De Tillieux, R. L. Knorr, R. Lipowsky and R. Dimova, *Sci. Rep.*, 2018, **8**, 11838.
14 J. Agudo-Canalejo and R. Lipowsky, *ACS Nano*, 2015, **9**, 3704–3720.
15 R. B. Lira, T. Robinson, R. Dimova and K. A. Riske, *Biophys. J.*, 2019, **116**, 79–91.
16 C. Bao, G. Pähler, B. Geil and A. Janshoff, *J. Am. Chem. Soc.*, 2013, **135**, 12176–12179.
17 (*a*) B. D. Plouffe, S. K. Murthy and L. H. Lewis, *Rep. Prog. Phys.*, 2014, **78**, 016601; (*b*) A. Ito, M. Shinkai, H. Honda and T. Kobayashi, *J. Biosci. Bioeng.*, 2005, **100**, 1–11.
18 Z. Liu, J. Cui and W. Zhan, *Soft Matter*, 2020, **16**, 2177–2184.
19 (*a*) M. Kumari, S. Rajak, S. P. Singh, S. I. Kumari, P. U. Kumar, U. S. N. Murty, M. Mahboob, P. Grover and M. F. Rahman, *J. Nanosci. Nanotechnol.*, 2012, **12**, 2149–2159; (*b*) T. R. Pisanic, J. D. Blackwell, V. I. Shubayev, R. R. Fiñones and S. Jin, *Biomaterials*, 2007, **28**, 2572–2581.
20 S. Eloul, W. C. K. Poon, O. Farago and D. Frenkel, *Phys. Rev. Lett.*, 2020, **124**, 188001.

Supplementary Information

## Controlled adhesion, membrane pinning and vesicle transport by Janus particles

Eleanor J. Ewins,[a†] Koohee Han,[b ‡] Bhuvnesh Bharti,[b§] Tom Robinson,[a] Orlin D. Velev[b] and Rumiana Dimova[a]*

a. Max Planck Institute of Colloids and Interfaces, Science Park Golm, 14476 Potsdam, Germany
b. Department of Chemical and Biomolecular Engineering, North Carolina State University, Raleigh, NC, USA
†Current address: Department of Biochemistry, Groningen Institute of Biomolecular Sciences & Biotechnology, University of Groningen, The Netherlands
‡Current address: Department of Chemical Engineering, Kyungpook National University, Daegu, Republic of Korea
§Current address: Cain Department of Chemical Engineering, Louisiana State University, Baton Rouge, LA 70803, USA
*Address correspondence to: e.j.ewins@rug.nl and rumiana.dimova@mpikg.mpg.de

**List of abbreviations**

AC – alternating current
BSA – bovine serum albumin
COM – centre of mass
DOPC - 1,2-dioleoyl-sn-glycero-3-phosphocholine
DOTAP - 1,2-dioleoyl-3-trimethylammonium-propane (chloride salt)
GUV – giant unilamellar vesicle
ITO – Indium tin oxide
LUV – large unilamellar vesicle
NA – numerical aperture
Rh-DPPE - 1,2-dipalmitoyl-sn-glycero-3-phosphoethanolamine-N- (lissamine rhodamine B sulfonyl) (Ammonium salt)
ROI – region of interest

**S1. Materials and methods**

*S1.1. Materials*.
1,2-dioleoyl-sn-glycero-3-phosphocholine (DOPC), 1,2-dioleoyl-3-trimethylammonium-propane (chloride salt) (DOTAP) and 1,2-dipalmitoyl-sn-glycero-3-phosphoethanolamine-N- (lissamine rhodamine B sulfonyl) (Ammonium salt) (Rh-DPPE) were acquired from Avanti Polar Lipids (Alabaster, AL); the lipid structures are given in Fig. S1. 100 nm pore diameter polycarbonate membranes were obtained from Whatman (Maidstone, UK). Indium tin oxide (ITO) coated glasses (ITO film thickness < 100 nm, resistance 50 Ω) were obtained from Präzisions Glas & Optik (Iserlohn, Germany). Glucose, sucrose, sodium chloride and bovine serum albumin (BSA) were all obtained from Sigma Aldrich (Darmstadt, Germany). The polystyrene particles used for direct adhesion to LUVs and GUVs (Polybead® microspheres, 6 μm non-functionalised polystyrene (exposed sulphate groups), 4 μm functionalised and non-functionalised (exposed amine or sulphate surface groups respectively)) were obtained from Polysciences (Germany). The uniform polystyrene particles used for Janus particle preparation were purchased from Bangs Lab Inc. (Indiana, USA). Iron and chromium pellets were purchased from Kurt J. Lesker Co. (Clairton, PA, USA).
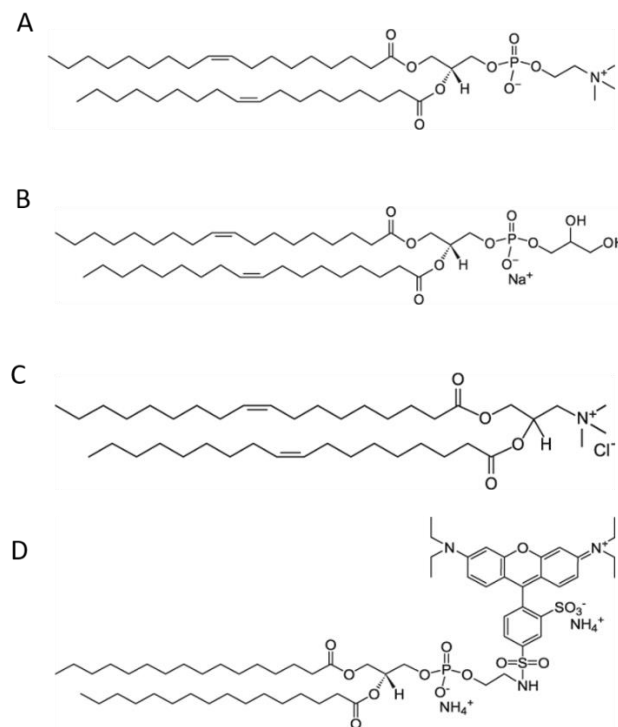
**Fig. S1** Structures of lipids used in this study. (A) 1,2-dioleoyl-sn-glycero-3-phosphocholine (DOPC). (B) 1,2-dioleoyl-sn-glycero-3-phospho-(1'-rac-glycerol) (sodium salt) (DOPG). (C) 1,2-dioleoyl-3-trimethylammonium-propane (chloride salt) (DOTAP). (D) 1,2-dipalmitoyl-sn-glycero-3-phosphoethanolamine-N-(lissamine rhodamine B sulfonyl) (ammonium salt) (Rh-DPPE). *Images from Avanti Polar Lipids.*

*S1.2. Vesicle preparation and mixing with particles.*

Large unilamellar vesicles (LUVs) were prepared via extrusion at room temperature.[1] The lipid solution was prepared to 2.2 mL in chloroform at a concentration of 2 mM and composed of either DOPC/DOTAP/Rh-DPPE (59.5/40/0.5 molar ratio), DOPC/DOPG/Rh-DPPE (59.5/40/0.5 molar ratio) or DOPC/DOTAP/Rh-DPPE (94.5/5/0.5 molar ratio) and deposited in a small glass vial. The chloroform was evaporated first under a stream of $N_2$ and then further dried under vacuum for 2 hours. The lipid film was then rehydrated with either 0.2 M sucrose or 150 mM NaCl to a final lipid concentration of 1.2 mM. The solution was vortexed for 2-5 minutes, obtaining multilamellar vesicles. The vesicle solution was then subjected to 11 cycles of extrusion through a 100 nm pore diameter polycarbonate membrane. For the adhesion studies, LUVs were mixed with the microspheres and incubated for 1 hour before imaging, in a vertical rotating mixer. The particles had a final concentration of $8.4 \times 10^4$ particles/mL and the LUVs had a final lipid concentration of 0.83 mg/mL.

Giant unilamellar vesicles (GUVs) were prepared via the established electroformation protocol.[2] Lipid solutions were prepared in chloroform at 4 mM with varying ratios of DOPC and DOTAP, as indicated throughout the text. Unless explicitly stated in the text, lipid solutions also contained 0.5 mol% Rh-DPPE fluorescent dye. A total volume of 16 µL of the lipid solution in chloroform was spread on two conductive ITO-coated glasses and dried under vacuum for 2 to 2.5 hours at room temperature. The ITO glasses, together with a rectangular Teflon spacer, were then assembled to form a chamber of 2 mL volume which was filled with 0.2 M sucrose. The chamber was then connected to a function generator which was used

to apply an AC field (1.2 V, 10 Hz) for 1.5 hours at room temperature (for the lipid compositions containing dyes, the electroformation was performed in the dark). The GUVs were then removed from the growth chamber via pipetting and diluted 1:1 in a 0.21 M glucose solution (unless otherwise stated in the main text) containing dispersed particles. GUV suspensions and glucose solutions were measured and the osmolarity adjusted (glucose only) using an osmometer (Osmomat 030, Gonotec, Germany) such that the particle solution had higher osmolarity by ~10 mOsm. The GUVs were incubated with the particles (final concentration of $8.4 \times 10^3$ particles/mL) for 1 hour in a vertical rotating mixer before observation.

*S1.3. Janus particle preparation.*
Iron-patched Janus microspheres were prepared from the uniform polystyrene particles using a metal vapour deposition technique,[3, 4] see sketch in Fig. S2A. Briefly, the polystyrene particles were concentrated and washed by centrifuging at 1500 ×*g* for 5 min and replacing the supernatant with MQ water; this was repeated 2-3 times. A convective assembly method was used to deposit particle monolayers on pre-cleaned glass slides.[5] The dried particle monolayers were coated with hemispherical patches of chromium followed by a layer of iron (5 nm and 20 nm respectively) in a metal evaporator (Cooke Vacuum Products, model CV302). The thickness of the evaporated metals was monitored using a Maxtek Inc. TM350 thickness monitor equipped with SC-101 sensor crystals. The particles were then gently scraped from the deposition surface and resuspended in Milli-Q water. A SEM image of Janus particles is shown in Fig. S2B. The microparticles were then washed 3 times in Milli-Q water, via repeated centrifugation and removal of supernatant, before use. Note that the iron patch on the surface of microspheres transforms to iron oxide ($Fe_2O_3$) upon their resuspension in an aqueous environment.[3] In some brightfield images (depending on the particle orientation), it is also possible to distinguish a region of the particle surface that is darker, which corresponds to the iron oxide cap, see Fig. S2C.
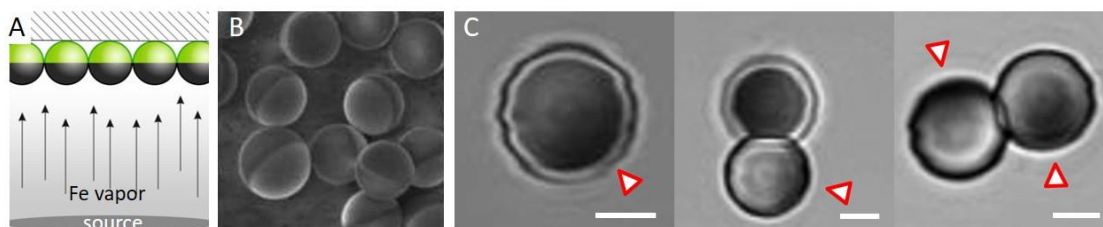


**Fig. S2** (A) Schematic of metal vapour deposition on a monolayer of polystyrene colloid spheres dried on a solid substrate, adapted from [4]. (B) SEM image of 4 µm Janus particles adapted from[3], clearly showing the two different surfaces on the same particle. (C) Brightfield images of 4 µm Janus particles in aqueous solution with visible darker patches (arrowheads pointing to them), corresponding to the iron oxide coating. Scale bars: 2 µm. The apparent distorted surface of the particle is an artefact of the slow scanning speed of the confocal microscope with which the images were acquired.

*S1.4. Imaging.*
Confocal imaging was performed on either a Leica confocal SP8 or SP5 setup (Mannheim, Germany). Rh-DPPE was excited with a 561 nm laser and the emission signal collected between 580-670 nm. The images were acquired with a 63x (1.2 NA) water immersion objective and 1 Airy unit. The subsequent image analysis is described in detail in section S2. Phase contrast imaging was performed on an Axio Observer

D1 (Zeiss, Germany) microscope, equipped with a Ph2 20x (NA 0.5) objective and an ORCA R2 CCD camera (Hamamatsu, Japan).

*S1.5. Magnetic manipulation of Janus particles.*

A handheld bar magnet was used to generate a magnetic field gradient by placing the magnet close (approximately 2 cm from pole of magnet to glass) to the observation chamber. The magnet is formed from multiple blocks of Neodymium (dimensions 2.0 cm × 2.0 cm × 10.4 cm), with an approximate total magnetic field of 1 mT (at the magnet surface). To change the direction of the magnetic field, the position of the magnet was rotated approximately 180° around the observation chamber. During image acquisition the magnet was held in a fixed position.

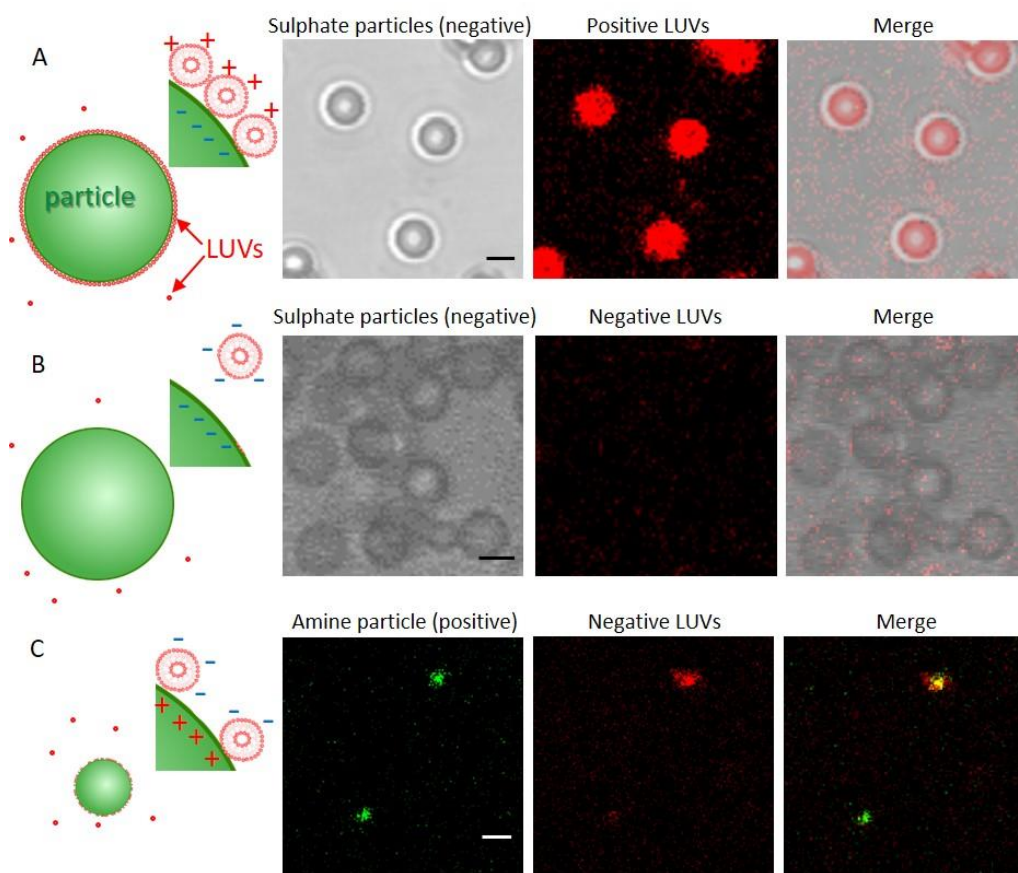**S2. Particle-membrane affinity with homogeneous and Janus particles**



**Fig. S3** Adhesion of fluorescently labelled LUVs of varying lipid compositions (and labelled with 0.5 mol% Rh-DPPE, red) to microparticles with different surface charges shown with schematic representations of the different degrees of interactions and bright-field and confocal images. The sketches roughly represent the relatively large size of the microparticles (6 μm or 1 μm) relative to that of the LUVs (100 nm). (A) 6 μm polystyrene particles with a negative surface charge (sulphate groups) and positively charged LUVs (DOPC/DOTAP 60/40 mol%). The LUVs (as observed from the fluorescence signal from the red dye Rh-DPPE in the membrane) completely cover the surface of all of the particles in the sample. (B) The same 6 μm polystyrene particles and negatively charged LUVs (DOPC/DOPG 60/40 mol%). The LUVs do not adhere

4

to the particles' surface, which we conclude from the lack of fluorescence signal in the particles' location in the merged image. (C) 1 μm polystyrene particles with amine functional groups (positively charged, labelled with green fluorescent dye) incubated with negatively charged LUVs (DOPC/DOPG 60/40 mol%, red) showed heterogeneous adhesion of LUVs to the particles' surfaces, as can be seen from the difference in fluorescence signals from the red LUVs on the two particles (middle image). All scale bars correspond to 5 μm. The merged images on the right show overlay of the signal detected in the channels showing the particles and the LUVs individually.
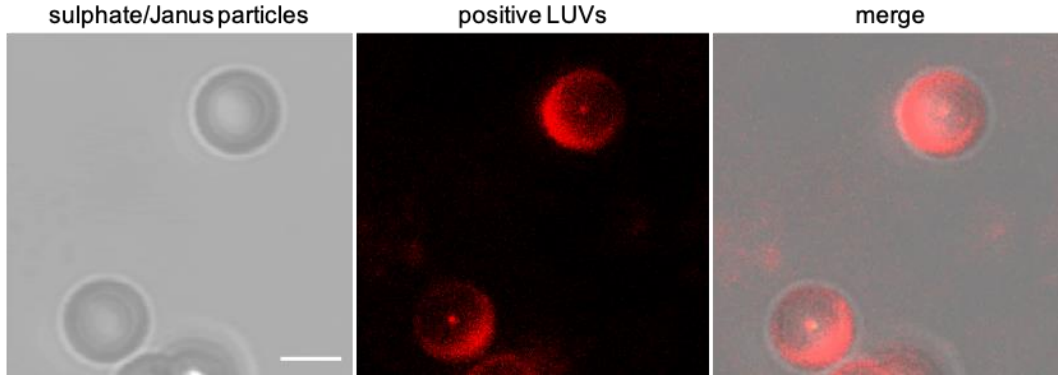


**Fig. S4** Preferential adhesion of LUVs to one region of Janus particles. DOTAP (positively charged) doped LUVs (labelled with Rh-DPPE visualized in red) only adhere to portions of Janus particle surfaces, indicating a stronger adhesion for one region compared to another. Scale bar: 3 μm. The non-adhesive region, exhibiting less fluorescence from the LUVs (middle image), corresponds to the metal patch, which appears darker in the brightfield image (left). The merged image shows an overlay of both.


**S3. Calculating particle penetration depth**

The particle penetration depth into the GUVs was calculated from a stack of confocal z-slices of each vesicle-particle pair. First, the (x,y) centre of mass ($COM_V$ in Fig. S5) of the vesicle was determined by fitting a circle to the vesicle contour in the z-stack with the largest diameter (the error on this value is the standard deviation of three such measurements on the same vesicle). The z-position of the COM(s) were calculated as the image number in the stack (e.g., z = 14) multiplied by the z step height (the error on this value was determined to be the z step height of the confocal stack, and is introduced when selecting the correct contour to measure). The centre of mass of the particle ($COM_P$) was determined in the same way from the brightfield channel. The distance between the vesicle COM and particle COM was calculated using Equation 1:

$$D = \left|\overrightarrow{COM_V COM_P}\right| = \sqrt{x^2 + y^2 + z^2} \tag{1}$$

in which $COM_V = [x_V, y_V, z_V]$, $COM_P = [x_P, y_P, z_P]$ and subsequently $x = x_V - x_P$ (and similarly for $y$ and $z$). The depth of particle penetration into the vesicle ($d$) is defined as the distance between the vesicle membrane on the particle surface (solid line in contact with particle) and where it is projected to be (dashed red line) if the particle were not present (by assuming the vesicle is spherical). This distance is therefore calculated using the following equation:

$$d = R_P + R_V - D \tag{2}$$

where $R_P$ and $R_V$ are the particle and vesicle radii respectively, as indicated in the diagram below.
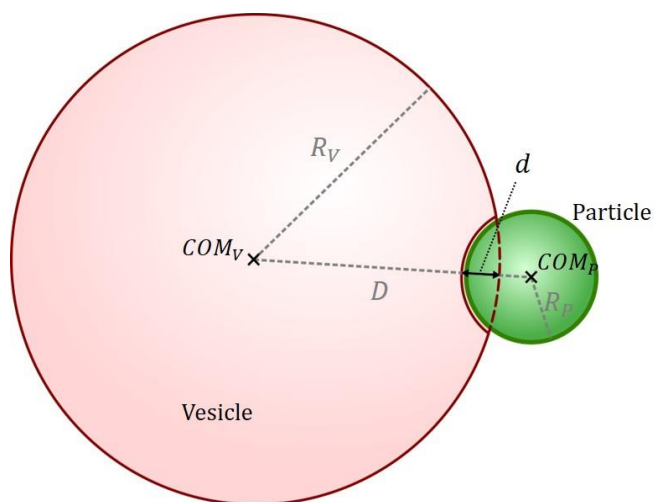


**Fig. S5** Schematic presentation of the vesicle and particle with indicated relevant dimensions of the system.

**S4. Imaging and evaluating LUV fluorescence on particle surface**
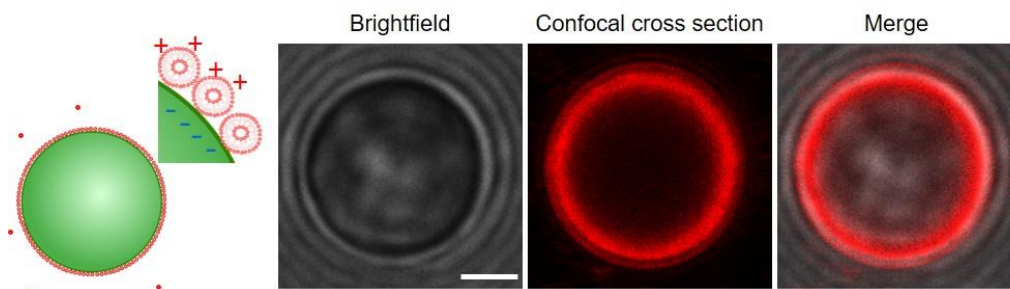


**Fig. S6** Brightfield and confocal cross-section with LUVs (red) adsorbed to the surface of a 6 μm polystyrene (sulphate surface groups, negative charge) particle (visible in brightfield image and overlay of the brightfield and red fluorescent channels) in the absence of salt. Scale bar 2 μm.
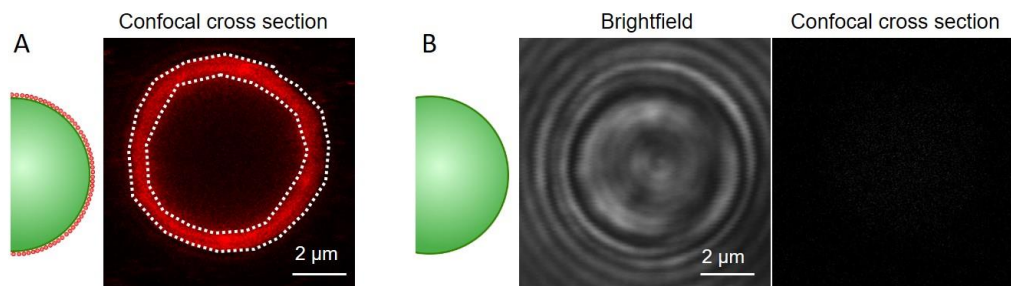


**Fig. S7** (A) Evaluating the fluorescently labelled LUV coverage on 6 μm polystyrene particles: a confocal cross section of one particle with dashed line indicating the ROI (region of interest) that is selected for fluorescence intensity analysis of LUV coverage. The analysis is carried out in LAS X, a confocal imaging

6

and analysis software from Leica. As the particles are roughly of the same size, the equatorial cross-section is imaged at the same height from the glass for all particles. When the ROI is selected, regions with visible lipid/vesicle aggregation (and thus higher intensity) are excluded from the selection. Example demonstrated here is for 200 mM sucrose (no salt). (B) Images taken at the same imaging settings and image brightness/contrast for comparison of particles in the absence of LUVs demonstrate that none of the fluorescence signal results from particle reflection or autofluorescence (there is no red signal in the confocal panel).
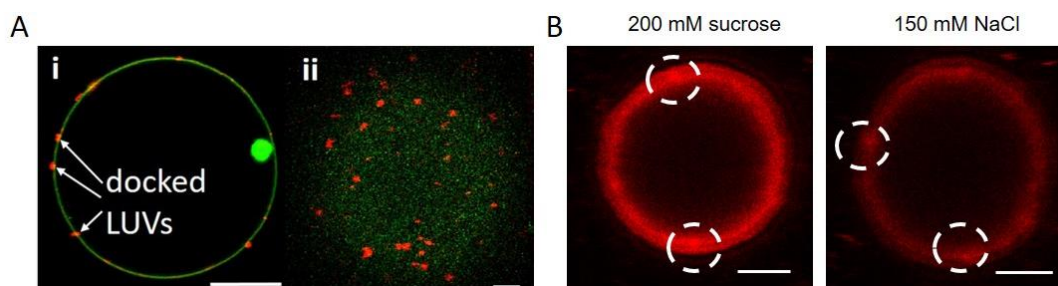


**Fig. S8 Comparison of LUVs fluorescence observed on GUV surface and on particle surface.** (A) Confocal images of LUVs docked on the surface of a GUV; (i) mid-plane confocal cross section of GUV (green) with docked LUVs (red) indicated and (ii) upper GUV surface. Images adapted from [6]. Scale bars (i) 10 μm, (ii) 2 μm. (B) Confocal image of LUVs present on the surface of a polystyrene particle in the conditions of Fig. 3 in the main text. Scale bars 2 μm. The fluorescence from individual docked LUVs (A) appear to produce stronger signal compared to the more homogeneous fluorescence that we observe over the particles (B), but certain spots of bright fluorescence (encircled in B) appear to result from LUV docking.


**Movie S1** Time series showing Janus particle adhered to a GUV moving through observation chamber in the presence of a magnetic field gradient; for details see Fig. 4 in the main text.

**References:**

1.      M. Riaz, *Pak J Pharm Sci*, 1996, **9**, 65-77.
2.      M. I. Angelova and D. S. Dimitrov, *Faraday Discuss. Chem. SOC*, 1986, **81**, 303-311.
3.      B. Bharti, D. Rutkowski, K. Han, A. U. Kumar, C. K. Hall and O. D. Velev, *Journal of the American Chemical Society*, 2016, **138**, 14948-14953.
4.      S. K. Smoukov, S. Gangwal, M. Marquez and O. D. Velev, *Soft Matter*, 2009, **5**, 1285-1292.
5.      B. G. Prevo and O. D. Velev, *Langmuir*, 2004, **20**, 2099-2107.
6.      R. B. Lira, T. Robinson, R. Dimova and K. A. Riske, *Biophysical Journal*, 2019, **116**, 79-91.